JPE 19-5-14

https://doi.org/10.6113/JPE.2019.19.5.1203
ISSN(Print): 1598-2092 / ISSN(Online): 2093-4718

# Fast Regulation Method for Commutation Shifts for Sensorless Brushless DC Motors

Xuliang Yao*, Jicheng Zhao†, and Jingfang Wang*

†,*College of Automation, Harbin Engineering University, Harbin, China

**Abstract**

Sensorless brushless DC (BLDC) motor drive systems are often subjected to inaccurate commutation signals and can produce high current peaks and conduction consumption. To achieve accurate commutation, a fast commutation shift regulation method for sensorless BLDC motor drive systems considering the influence of the inductance freewheeling process is presented to compensate inaccurate commutation signals. The regulation method is effective in both steady speed and variable speed operations. In the proposed method, the commutation error is gained from the line-voltage difference integral in a 60 electrical-degree conduction period and the outgoing phase current before commutation. In addition, the detection precision of the commutation error is improved due to the consideration of the freewheeling period. The commutation error is directly obtained, which avoids successive optimization and accelerates the convergence rate of the proposed method. Moreover, the commutation error features a positive or negative sign, which can be utilized as an indicator of advanced or delayed commutation. Finally, experiments are conducted to validate the effectiveness and feasibility of the proposed method. The results obtained show that the proposed method can accurately regulate commutation signals.

**Key words:** Brushless DC motor, Commutation error, Free-wheeling period, Sensorless drive

## I. INTRODUCTION

Brushless DC (BLDC) motors are widely used in the aerospace industry, electric vehicles and household applications due to their inherent advantages including high power density, high efficiency and simplicity in structure [1]-[3]. Rotor position information is important in motor control. Position sensors, such as hall-effect sensors, are generally used to acquire rotor position signals for proper commutation. However, hall-effect sensors are susceptible to electromagnetic interference and high-temperature surroundings, which can eventually lead to inaccurate rotor position signals. Disturbed position information deviates motors from accurate commutation instants, which results in high current peaks and conduction loss [4]-[6].

Many sensorless drive techniques have been investigated to obtain accurate rotor position signals for overcoming the above-mentioned drawbacks. Among these strategies, the zero-crossing points (ZCPs) of back electromotive force (back-EMF) are easily detected and widely adopted in position sensorless control. The ZCPs of back-EMF are often abstracted from the terminal voltage. However, the terminal voltage is vulnerable to high-frequency components due to pulse-width modulation (PWM) switching. A low-pass filter is usually applied to remove the high-frequency switching noise of the terminal voltage. However, it also introduces a phase delay for the ZCP detection of back-EMF. In [7], a hysteresis comparator is used to compensate phase delay. However, it requires offline compensation, and the compensation rate is limited. The floating phase terminal voltage during the PWM off time is used to directly detect the ZCPs of back-EMF without a low-pass filter [8]. However, it is unsuitable in the low speed range. The authors of [9] proposed a dynamic rate limiter to identify the ZCPs of zero-sequence voltage. However, the parameter of the rate limiter needs to be elaborately adjusted. In [10], the authors analyzed the commutation error in traditional line-to-line voltage ZCP detection and proposed a two-stage commutation error correction method for both high-speed and low-speed applications. Nevertheless, this method adds additional hardware circuits and has poor stability.

Various estimation and observer methods have been presented to achieve accurate commutation [11]-[19]. In [11],

Manuscript received Dec. 11, 2018; accepted Apr. 17, 2019
Recommended for publication by Associate Editor Wook-Jin Lee.
†Corresponding Author: worryfree@126.com
Tel: +86-13059035611, Harbin Engineering University
*College of Automation, Harbin Engineering University, China

the authors used the torque constant as a reference signal of the position detection to obtain accurate commutation signals. In [12], the rotor position is required from back-EMF difference, which is estimated from a disturbance observer structure. Estimation methods based on sliding-mode observers [13], [14], Kalman filters [15]-[17], and extended Kalman filters [18], [19] have been adopted to accurately extract information of rotor position. However, the algorithms are complicated and require a large number of calculations.

To improve the precision of commutation signals, some commutation instant regulation methods have been proposed in recent years. In [20], an intelligent self-tuning strategy was presented to finely adjust commutation instants. In addition, the regulation of the commutation instants is realized by minimizing the stator current. In [21], the commutation errors are adjusted by forcing the dc-link current difference to zero before and after commutation instants. However, this method is based on a linearized approximation between the DC-link current difference and the commutation time error. In [22], the commutation errors are compensated by keeping the freewheeling current of the unenergized phase symmetrical. When dealing with some PWM strategies featuring the suppression of freewheeling current, this method is unsuitable. In addition, this method is accomplished by successive optimization, resulting in slow response of the regulation. In [23], the symmetrical characteristics of unenergized phase terminal voltage are presented to regulate commutation instants. However, the effects of the freewheeling period are not considered. In [24], the commutation error is compensated by a PI regulator, which inevitably prolongs the regulation time of the commutation error.

In this paper, a fast commutation shift regulation method is presented to adjust the commutation signals of sensorless BLDC motors. In this method, the commutation error is calculated with the line voltage difference integral value in 60 electrical degrees and the outgoing phase current before commutation. Then it is directly applied to adjust inaccurate commutation signals. The sign of the commutation error is employed to judge advanced or delayed commutation. In the practical implementation, the error sources are inevitable and they can produce commutation errors. In [25], the commutation error cannot be gained and is regulated with a PI controller which extends the regulation time of the commutation error. But the commutation error in the proposed method is directly obtained and the commutation error is immediately compensated in the next adjacent period which avoids progressive optimization and accelerates convergence rate. In addition, the proposed method is less sensitive to switching noise so that the accuracy is improved.

The remainder of this paper is organized as follows. A mathematical model of a BLDC motor is described in Section II. The commutation shift regulation method is proposed in Section III. Experimental results to support the validity and effectiveness of the proposed method are provided in Section IV. Some conclusions are presented in Section V.

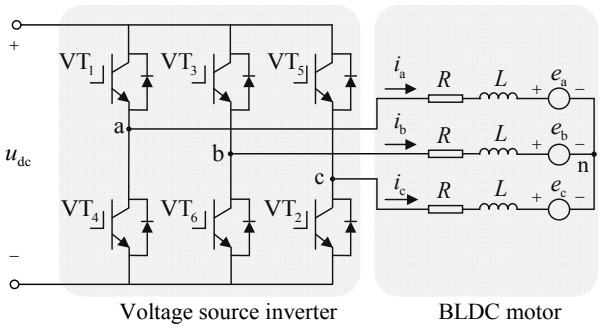


Fig. 1. Equivalent circuit of a BLDC motor drive system.

## II. Mathematical Model of a BLDC Motor

An equivalent circuit of a BLDC motor drive system is shown in Fig. 1. In this paper, a surface-mounted permanent-magnet rotor structure is considered. It is assumed that the voltage drop of each of the controllable switches is equal, the three-phase stator windings are symmetrical, the phase resistance and inductance are constant, and the armature reaction is negligible. The voltage equations are described as:

$$\begin{bmatrix} u_a \\ u_b \\ u_c \end{bmatrix} = \begin{bmatrix} R & 0 & 0 \\ 0 & R & 0 \\ 0 & 0 & R \end{bmatrix} \begin{bmatrix} i_a \\ i_b \\ i_c \end{bmatrix} + \begin{bmatrix} L & 0 & 0 \\ 0 & L & 0 \\ 0 & 0 & L \end{bmatrix} \frac{d}{dt} \begin{bmatrix} i_a \\ i_b \\ i_c \end{bmatrix} + \begin{bmatrix} e_a \\ e_b \\ e_c \end{bmatrix} + \begin{bmatrix} u_n \\ u_n \\ u_n \end{bmatrix} \quad (1)$$

where $u_a$, $u_b$ and $u_c$ are the three-phase voltages, $i_a$, $i_b$ and $i_c$ are the three-phase currents, $e_a$, $e_b$ and $e_c$ are the phase back-EMFs, $R$ is the stator resistance, $L$ is the phase inductance, and $u_n$ is the neutral voltage.

The line voltage equations of a BLDC motor drive system are described as:

$$\begin{cases} u_{ab} = u_a - u_b = R(i_a - i_b) + Ld(i_a - i_b)/dt + e_a - e_b \\ u_{bc} = u_b - u_c = R(i_b - i_c) + Ld(i_b - i_c)/dt + e_b - e_c \\ u_{ca} = u_c - u_a = R(i_c - i_a) + Ld(i_c - i_a)/dt + e_c - e_a \end{cases} \quad (2)$$

## III. Proposed Commutation Shift Regulation Method

Under the influence of the rotor magnetic structure, armature reaction, magnetization unbalance of the permanent magnets, manufacturing errors and design compatibility, it is not easy to gain an ideal trapezoidal air-gap flux distribution. Generally, the flat-top width of the back-EMF is less than 120°. Fig. 2 shows a phase diagram of the back-EMF and commutation signals, where $\beta$ is the phase deviation from one side of the flat-top back-EMF. $L_a$, $L_b$ and $L_c$ are the commutation signals. $\alpha$ denotes the absolute value of the commutation error $\varphi$ between the actual commutation position and the accurate commutation position, and it is

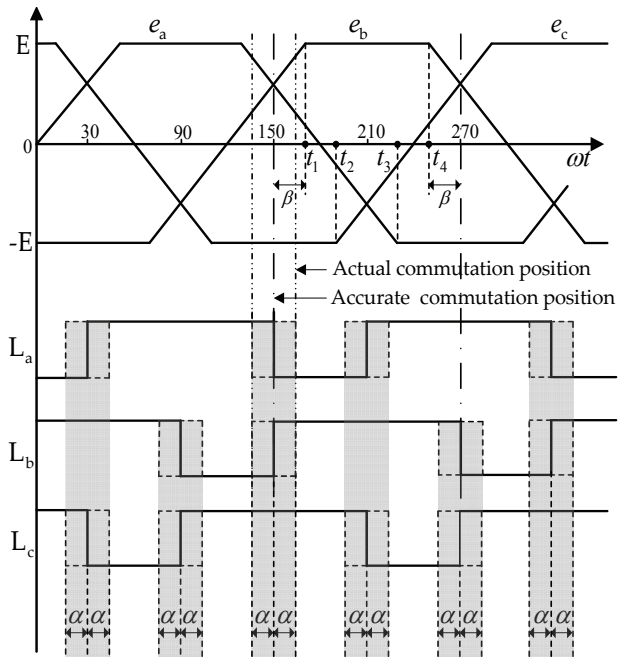


Fig. 2. Phase diagram of back-EMF and commutation signals.

assumed that the commutation error $\varphi \in [-30^{\circ}, 30^{\circ}]$. In addition, $t_1$, $t_2$, $t_3$, and $t_4$ are the boundary points of the flat-top back-EMF.

### *A. Without Consideration of the Freewheeling Process*

*1) Delayed Commutation*: At a particular step, assume that $VT_3$ and $VT_2$ are conducting, and that $VT_1$ is floating. When the commutation instants are delayed by $\alpha$, the conduction of $VT_3$ and $VT_2$ lasts a period when $t \in \left[t_{150^{\circ}+\alpha}, t_{210^{\circ}+\alpha}\right]$, as shown in Fig. 2. During $t \in \left[t_{150^{\circ}+\alpha}, t_{210^{\circ}+\alpha}\right]$, the line voltage difference integral during a 60-degree conduction period can be expressed as:

$$\int_{t_{150^{\circ}+\alpha}}^{t_{210^{\circ}+\alpha}} \left(u_{ca} - u_{ab}\right) dt = \int_{t_{150^{\circ}+\alpha}}^{t_{210^{\circ}+\alpha}} A_{z1} dt + \int_{t_{150^{\circ}+\alpha}}^{t_{210^{\circ}+\alpha}} A_{e1} dt \tag{3}$$

where: $\begin{aligned} A_{z1} &= R(i_b + i_c - 2i_a) + Ld\left(i_b + i_c - 2i_a\right)/dt \\ A_{e1} &= e_b + e_c - 2e_a \end{aligned}$.

Considering a BLDC motor with a negligible freewheeling period $t_{fw}$, the current satisfies $i_b = -i_c$ and $i_a = 0$ during the entire 60-electrical degree period when $t \in \left[t_{150^{\circ}+\alpha}, t_{210^{\circ}+\alpha}\right]$. Therefore, it meets $A_{z1}=0$, and the line voltage difference integral $\int_{t_{150^{\circ}+\alpha}}^{t_{210^{\circ}+\alpha}} \left(u_{ca} - u_{ab}\right) dt$ is simplified as:

$$\int_{t_{150^{\circ}+\alpha}}^{t_{210^{\circ}+\alpha}} \left(u_{ca} - u_{ab}\right) dt = \int_{t_{150^{\circ}+\alpha}}^{t_{210^{\circ}+\alpha}} A_{e1} dt \tag{4}$$

According to the back-EMFs shown in Fig. 2, non-ideal back-EMFs during $t \in \left[t_{150^{\circ}+\alpha}, t_{210^{\circ}+\alpha}\right]$ can be expressed as:

$$\begin{aligned} e_a &= -\frac{6K_e\omega}{\pi + 6\beta} \cdot \omega \cdot \left(t - t_{180}\right), && t_{150^{\circ}+\alpha} \le t < t_{210^{\circ}+\alpha} \\ e_b &= \begin{cases} K_e\omega - \dfrac{6K_e\omega}{\pi + 6\beta} \cdot \omega \cdot \left(t_1 - t\right), & t_{150^{\circ}+\alpha} \le t < t_1 \\ K_e\omega, & t_1 \le t < t_{210^{\circ}+\alpha} \end{cases} \\ e_c &= \begin{cases} -K_e\omega, & t_{150^{\circ}+\alpha} \le t < t_2 \\ -K_e\omega + \dfrac{6K_e\omega}{\pi + 6\beta} \cdot \omega \cdot (t - t_2), & t_2 \le t < t_{210^{\circ}+\alpha} \end{cases} \end{aligned} \tag{5}$$

where $K_e$ is the efficiency of the back-EMF, and $\omega$ is the angular speed of the motor.

By substituting (5) into (4), the line voltage difference integral $\int_{t_{150^{\circ}+\alpha}}^{t_{210^{\circ}+\alpha}} \left(u_{ca} - u_{ab}\right) dt$ is shown as:

$$\begin{aligned} &\int_{t_{150^{\circ}+\alpha}}^{t_{210^{\circ}+\alpha}} \left(u_{ca} - u_{ab}\right) dt = \int_{t_{150^{\circ}+\alpha}}^{t_{210^{\circ}+\alpha}} (e_b + e_c - 2e_a) dt \\ &= \int_{t_{150^{\circ}+\alpha}}^{t_1} \left[K_e\omega - \frac{6K_e\omega}{\pi + 6\beta} \times \omega \times \left(t_1 - t\right)\right] dt + \int_{t_1}^{t_{210^{\circ}+\alpha}} K_e\omega dt \\ &+ \int_{t_{150^{\circ}+\alpha}}^{t_2} \left(-K_e\omega\right) dt + \int_{t_2}^{t_{210^{\circ}+\alpha}} \left[-K_e\omega + \frac{6K_e\omega}{\pi + 6\beta} \times \omega \times (t - t_2)\right] dt \\ &-2\int_{t_{150^{\circ}+\alpha}}^{t_{210^{\circ}+\alpha}} \left[-\frac{6K_e\omega}{\pi + 6\beta} \times \omega \times \left(t - t_{180}\right)\right] dt = \frac{4\alpha K_e\left(3\beta + \pi\right)}{p\left(\pi + 6\beta\right)} \end{aligned} \tag{6}$$

where $p$ is the number of pole pairs.

By rearranging (6), the commutation error $\varphi$ under a delayed commutation can be expressed as:

$$\varphi = \frac{\int_{t_{150^{\circ}+\alpha}}^{t_{210^{\circ}+\alpha}} \left(u_{ca} - u_{ab}\right) dt}{C_e} = \alpha > 0 \tag{7}$$

where $C_e = 4K_e\left(3\beta + \pi\right) / p\left(\pi + 6\beta\right)$.

*2) Advanced Commutation:* When commutation instants are advanced by $\alpha$, the conduction of $VT_3$ and $VT_2$ lasts a period when $t \in \left[t_{150^{\circ}-\alpha}, t_{210^{\circ}-\alpha}\right]$, as shown in Fig. 2. The line voltage difference integral during the 60-degree conduction period can be expressed as:

$$\int_{t_{150^{\circ}-\alpha}}^{t_{210^{\circ}-\alpha}} \left(u_{ca} - u_{ab}\right) dt = \int_{t_{150^{\circ}-\alpha}}^{t_{210^{\circ}-\alpha}} A_{e2} dt \tag{8}$$

where $A_{e2} = e_b + e_c - 2e_a$.

Similarly, the back-EMFs during $t \in \left[t_{150^{\circ}-\alpha}, t_{210^{\circ}-\alpha}\right]$ can be expressed as:

$$\begin{aligned} e_a &= -\frac{6K_e\omega}{\pi + 6\beta} \cdot \omega \cdot \left(t - t_{180}\right), && t_{150^{\circ}-\alpha} \le t < t_{210^{\circ}-\alpha} \\ e_b &= \begin{cases} K_e\omega - \dfrac{6K_e\omega}{\pi + 6\beta} \cdot \omega \cdot \left(t_1 - t\right), & t_{150^{\circ}-\alpha} \le t < t_1 \\ K_e\omega, & t_1 \le t < t_{210^{\circ}-\alpha} \end{cases} \\ e_c &= \begin{cases} -K_e\omega, & t_{150^{\circ}-\alpha} \le t < t_2 \\ -K_e\omega + \dfrac{6K_e\omega}{\pi + 6\beta} \cdot \omega \cdot (t - t_2), & t_2 \le t < t_{210^{\circ}-\alpha} \end{cases} \end{aligned} \tag{9}$$

By substituting (9) into (8), the line voltage difference integral $\int_{t_{150°-\alpha}}^{t_{210°-\alpha}}(u_{ca}-u_{ab})dt$ is shown as:

$$\begin{aligned}&\int_{t_{150°-\alpha}}^{t_{210°-\alpha}}(u_{ca}-u_{ab})dt=\int_{t_{150°-\alpha}}^{t_{210°-\alpha}}(e_b+e_c-2e_a)dt\\&=\int_{t_{150°-\alpha}}^{t_1}\left[K_e\omega-\frac{6K_e\omega}{\pi+6\beta}\cdot\omega\cdot(t_1-t)\right]dt+\int_{t_1}^{t_{210°-\alpha}}K_e\omega dt\\&+\int_{t_{150°-\alpha}}^{t_2}(-K_e\omega)dt+\int_{t_2}^{t_{210°-\alpha}}\left[-K_e\omega+\frac{6K_e\omega}{\pi+6\beta}\cdot\omega\cdot(t-t_2)\right]dt\\&-2\int_{t_{150°-\alpha}}^{t_{210°-\alpha}}\left[-\frac{6K_e\omega}{\pi+6\beta}\cdot\omega\cdot(t-t_{180})\right]dt=\frac{-4\alpha K_e(3\beta+\pi)}{p(\pi+6\beta)}\end{aligned}\tag{10}$$

By rearranging (10), the commutation error $\varphi$ under advanced commutation can be expressed as:

$$\varphi=\frac{\int_{t_{150°-\alpha}}^{t_{210°-\alpha}}(u_{ca}-u_{ab})dt}{C_e}=-\alpha<0\tag{11}$$

where $\alpha$ denotes the absolute value of the commutation error $\varphi$ between the actual commutation position and the accurate commutation position.

Therefore, the commutation error $\varphi$ during the conduction period of $VT_3$ and $VT_2$ can be shown as:

$$\varphi=\begin{cases}\dfrac{\int_{t_{150°+\alpha}}^{t_{210°+\alpha}}(u_{ca}-u_{ab})dt}{C_e}=\alpha>0\\(\text{Delayed commutation}),\\\dfrac{\int_{t_{150°-\alpha}}^{t_{210°-\alpha}}(u_{ca}-u_{ab})dt}{C_e}=-\alpha<0\\(\text{Advanced commutation})\end{cases}\tag{12}$$

During a second 60-degree conduction period of $VT_3$, $VT_3$ and $VT_4$ are conducting. The commutation error $\varphi$ under delayed and advanced commutations can be expressed as:

$$\varphi=\begin{cases}\dfrac{\int_{t_{210°+\alpha}}^{t_{270°+\alpha}}(u_{bc}-u_{ca})dt}{C_e}=-\alpha<0\\(\text{Delayed commutation}),\\\dfrac{\int_{t_{210°-\alpha}}^{t_{270°-\alpha}}(u_{bc}-u_{ca})dt}{C_e}=\alpha>0\\(\text{Advanced commutation})\end{cases}\tag{13}$$

According to the previous analysis, the general function of the commutation error $\varphi$ is given as:

$$\varphi=\left(\int_{t_s}^{t_e}(u_{xz}-u_{zy})dt\right)\Big/C_e\tag{14}$$

where the subscripts x and y represent the active phases, and z represents the inactive phase. $t_s$ and $t_e$ represent the lower limit and upper limits of the integration, respectively.

TABLE I
RELATIONSHIP BETWEEN COMMUTATION ERRORS AND COMMUTATION INFORMATION

| Conduction Switch | Commutation Error $\varphi$ | Sign ($\varphi$) | Advanced /Delayed |
|---|---|---|---|
| $VT_1$-$VT_6$ | $\left(\int_{t_s}^{t_e}(u_{bc}-u_{ca})dt\right)/C_e$ | $>0$ | Delayed |
| | | $<0$ | Advanced |
| $VT_1$-$VT_2$ | $\left(\int_{t_s}^{t_e}(u_{ab}-u_{bc})dt\right)/C_e$ | $<0$ | Delayed |
| | | $>0$ | Advanced |
| $VT_3$-$VT_2$ | $\left(\int_{t_s}^{t_e}(u_{ca}-u_{ab})dt\right)/C_e$ | $>0$ | Delayed |
| | | $<0$ | Advanced |
| $VT_3$-$VT_4$ | $\left(\int_{t_s}^{t_e}(u_{bc}-u_{ca})dt\right)/C_e$ | $<0$ | Delayed |
| | | $>0$ | Advanced |
| $VT_5$-$VT_4$ | $\left(\int_{t_s}^{t_e}(u_{ab}-u_{bc})dt\right)/C_e$ | $>0$ | Delayed |
| | | $<0$ | Advanced |
| $VT_5$-$VT_6$ | $\left(\int_{t_s}^{t_e}(u_{ca}-u_{ab})dt\right)/C_e$ | $<0$ | Delayed |
| | | $>0$ | Advanced |

From (12) and (13), the commutation error $\varphi$ can be directly obtained and it features different polarities under advanced and delayed commutations. Hence, the sign of the commutation error $\varphi$ can be used as an indicator of an advanced or delayed commutation.

The relationships among the conduction switch, commutation error and commutation information (delayed or advanced commutation) are shown in Table I.

### *B. With Consideration of the Freewheeling Process*

*1) Delayed Commutation:* Likewise, the conduction period of $VT_3$ and $VT_2$ is taken as an example. The commutation instants are delayed by $\alpha$, and the phase current is shown Fig. 3(a). The line voltage difference integral during the 60-degree conduction period can be expressed as:

$$\int_{t_{150°+\alpha}}^{t_{210°+\alpha}}(u_{ca}-u_{ab})dt=\int_{t_{150°+\alpha}}^{t_{210°+\alpha}}A_{z1}dt+\int_{t_{150°+\alpha}}^{t_{210°+\alpha}}A_{e1}dt\tag{15}$$

When the freewheeling process of the phase inductance is considered, the impact of $A_{z1}$ cannot be ignored.

In a 60-degree conduction period, two periods are included according to the winding conduction state: the freewheeling period and the normal conduction period. In the freewheeling period, when $t\in[t_{150°+\alpha},t_{150°+\alpha}+t_{fw}]$, the outgoing current $i_a$ gradually vanishes, the active current $i_b$ begins to rise, and the un-commutated current $i_c$ continues conducting, where $t_{fw}$ represents the free-wheeling period of the outgoing phase current.

During the freewheeling period, the three-phase current is simultaneously conducting, and the phase current equation meets $i_a+i_b+i_c=0$. In the normal conduction period, when $t\in[t_{150°+\alpha}+t_{fw},t_{210°+\alpha}]$, the phase currents $i_b$ and $i_c$ conduct and the outgoing phase current $i_a$ remains zero. The phase current equations meet $i_a=0$, $i_b+i_c=0$. The integral item $\int_{t_{150°+\alpha}}^{t_{210°+\alpha}}A_{z1}\mathrm{d}t$ for the voltage-drop sum of the inductance and

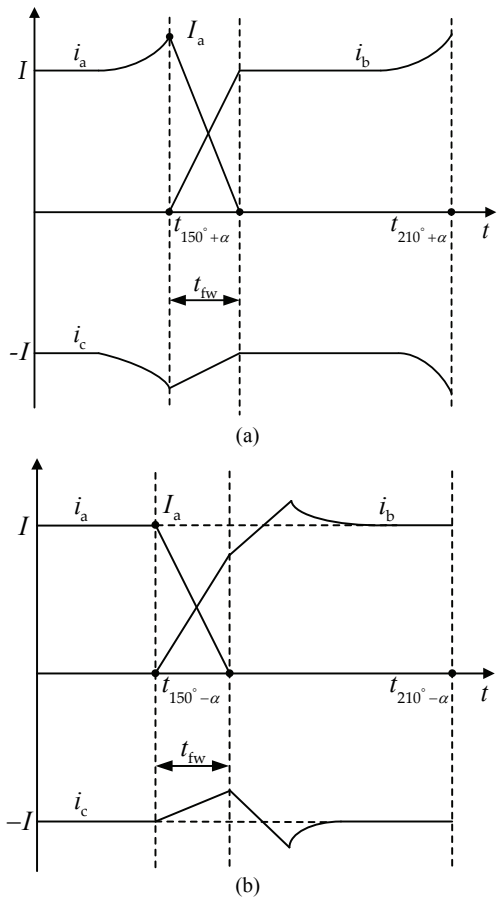


Fig. 3. Phase current when $VT_3$ and $VT_2$ are conducting. (a) Delayed commutation. (b) Advanced commutation.

resistance can be expressed as:

$$\begin{aligned}&\int_{t_{150^\circ+\alpha}}^{t_{210^\circ+\alpha}} A_{z1}dt\\&=\int_{t_{150^\circ+\alpha}}^{t_{150^\circ+\alpha}+t_{fw}}\left[R(i_b+i_c-2i_a)+Ld\left(i_b+i_c-2i_a\right)/dt\right]dt\\&+\int_{t_{150^\circ+\alpha}+t_{fw}}^{t_{210^\circ+\alpha}}\left[R(i_b+i_c-2i_a)+Ld\left(i_b+i_c-2i_a\right)/dt\right]dt\\&=-3\int_{t_{150^\circ+\alpha}}^{t_{150^\circ+\alpha}+t_{fw}}\left[Ri_a+Ldi_a/dt\right]dt\end{aligned}\tag{16}$$

Given that $R\int_{t_{150^\circ+\alpha}}^{t_{150^\circ+\alpha}+t_{fw}} i_a dt$ is far less than $LI_a$, the effect of the phase resistance is negligible, and (16) can be simplified as:

$$\int_{t_{150^\circ+\alpha}}^{t_{210^\circ+\alpha}} A_{z1}dt=\int_{t_{150^\circ+\alpha}}^{t_{150^\circ+\alpha}+t_{fw}}\left[-3Ldi_a/dt\right]dt=3LI_a\tag{17}$$

where $I_a$ is the final value of the outgoing phase current before commutation.

By combining (6), (15) and (17), the commutation error $\varphi$ under delayed commutation is solved as:

$$\varphi=\frac{\int_{t_{150^\circ+\alpha}}^{t_{210^\circ+\alpha}}\left(u_{ca}-u_{ab}\right)dt-3LI_a}{C_e}=\alpha>0\tag{18}$$

*2) Advanced Commutation:* Fig. 3(b) shows the phase current under advanced commutation. The line voltage difference integral during the a 60-degree conduction period can be expressed as:

$$\int_{t_{150^\circ-\alpha}}^{t_{210^\circ-\alpha}}\left(u_{ca}-u_{ab}\right)dt=\int_{t_{150^\circ-\alpha}}^{t_{210^\circ-\alpha}}A_{z2}dt+\int_{t_{150^\circ-\alpha}}^{t_{210^\circ-\alpha}}A_{e2}dt\tag{19}$$

When $t\in\left[t_{150^\circ-\alpha},t_{210^\circ-\alpha}\right]$, the phase current equations during the normal conduction period and the freewheeling period are the same as those under delayed commutation. According to the same analysis mentioned under delayed commutation, the integral item $\int_{t_{150^\circ-\alpha}}^{t_{210^\circ-\alpha}}A_{z2}dt$ for the voltage-drop sum of the inductance and resistance can be expressed as:

$$\begin{aligned}&\int_{t_{150^\circ-\alpha}}^{t_{210^\circ-\alpha}}A_{z2}dt\\&=\int_{t_{150^\circ-\alpha}}^{t_{150^\circ-\alpha}+t_{fw}}\left[R(i_b+i_c-2i_a)+Ld\left(i_b+i_c-2i_a\right)/dt\right]dt\\&+\int_{t_{150^\circ-\alpha}+t_{fw}}^{t_{210^\circ-\alpha}}\left[R(i_b+i_c-2i_a)+Ld\left(i_b+i_c-2i_a\right)/dt\right]dt\\&=3LI_a\end{aligned}\tag{20}$$

By combining (10), (19) and (20), the commutation error $\varphi$ can be solved as:

$$\varphi=\frac{\int_{t_{150^\circ-\alpha}}^{t_{210^\circ-\alpha}}\left(u_{ca}-u_{ab}\right)dt-3LI_a}{C_e}=-\alpha<0\tag{21}$$

Therefore, the commutation error $\varphi$ during the conduction period of $VT_3$ and $VT_2$ can be shown as:

$$\varphi=\begin{cases}\dfrac{\int_{t_{150^\circ+\alpha}}^{t_{210^\circ+\alpha}}\left(u_{ca}-u_{ab}\right)dt-3LI_a}{C_e}=\alpha>0\\\left(\text{Delayed commutation}\right),\\\dfrac{\int_{t_{150^\circ-\alpha}}^{t_{210^\circ-\alpha}}\left(u_{ca}-u_{ab}\right)dt-3LI_a}{C_e}=-\alpha<0\\\left(\text{Advanced commutation}\right)\end{cases}\tag{22}$$

During the second 60-degree conduction period of $VT_3$, $VT_3$ and $VT_4$ are conducting. The commutation error $\varphi$ under delayed and advanced commutations can be expressed as:

$$\varphi=\begin{cases}\dfrac{\int_{t_{210^\circ+\alpha}}^{t_{270^\circ+\alpha}}\left(u_{bc}-u_{ca}\right)dt-3LI_c}{C_e}=-\alpha<0\\\left(\text{Delayed commutation}\right),\\\dfrac{\int_{t_{210^\circ-\alpha}}^{t_{270^\circ-\alpha}}\left(u_{bc}-u_{ca}\right)dt-3LI_c}{C_e}=\alpha>0\\\left(\text{Advanced commutation}\right)\end{cases}\tag{23}$$

When the freewheeling process of the phase inductance is considered, the general function of the commutation error $\varphi$ is updated as:

TABLE II
RELATIONSHIP BETWEEN COMMUTATION ERRORS AND COMMUTATION INFORMATION

| Conduction Switch | Commutation Error $\varphi$ | Sign ($\varphi$) | Advanced/Delayed |
|---|---|---|---|
| $VT_1$-$VT_6$ | $\left(\int_{t_s}^{t_e}(u_{bc}-u_{ca})dt-3LI_c\right)/C_e$ | >0 | Delayed |
| | | <0 | Advanced |
| $VT_1$-$VT_2$ | $\left(\int_{t_s}^{t_e}(u_{ab}-u_{bc})dt-3LI_b\right)/C_e$ | <0 | Delayed |
| | | >0 | Advanced |
| $VT_3$-$VT_2$ | $\left(\int_{t_s}^{t_e}(u_{ca}-u_{ab})dt-3LI_a\right)/C_e$ | >0 | Delayed |
| | | <0 | Advanced |
| $VT_3$-$VT_4$ | $\left(\int_{t_s}^{t_e}(u_{bc}-u_{ca})dt-3LI_c\right)/C_e$ | <0 | Delayed |
| | | >0 | Advanced |
| $VT_5$-$VT_4$ | $\left(\int_{t_s}^{t_e}(u_{ab}-u_{bc})dt-3LI_b\right)/C_e$ | >0 | Delayed |
| | | <0 | Advanced |
| $VT_5$-$VT_6$ | $\left(\int_{t_s}^{t_e}(u_{ca}-u_{ab})dt-3LI_a\right)/C_e$ | <0 | Delayed |
| | | >0 | Advanced |

TABLE III
PREDEFINED COMMUTATION SEQUENCES

| $\hat{H}_a\ \hat{H}_b\ \hat{H}_c$ | 001 | 101 | 100 | 110 | 010 | 011 |
|---|---|---|---|---|---|---|
| Direction | Clockwise | | | | | |
| Conduction Switch | $VT_3$-$VT_2$ | $VT_3$-$VT_4$ | $VT_5$-$VT_4$ | $VT_5$-$VT_6$ | $VT_1$-$VT_6$ | $VT_1$-$VT_2$ |
| Direction | Anti-Clockwise | | | | | |
| Conduction Switch | $VT_5$-$VT_6$ | $VT_1$-$VT_6$ | $VT_1$-$VT_2$ | $VT_3$-$VT_2$ | $VT_3$-$VT_4$ | $VT_5$-$VT_4$ |

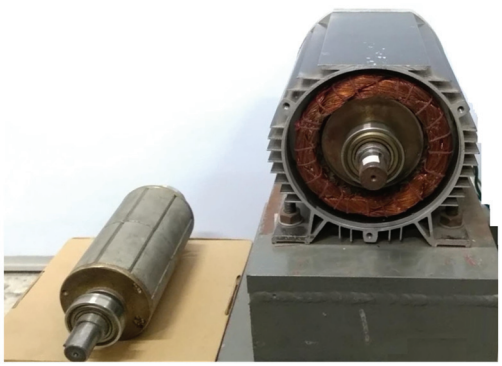

Fig. 4. Structure of the employed BLDC motor.

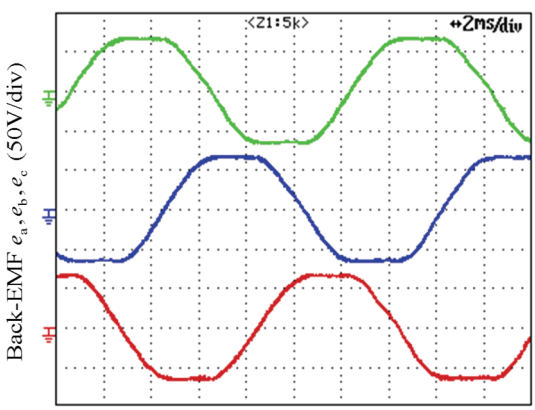


Fig. 5. Measured back-EMF of a BLDC motor at 1200r/min.

$$\varphi=\left(\int_{t_s}^{t_e}\left(u_{xz}-u_{zy}\right)dt-3LI_z\right)\Big/C_e \tag{24}$$

The relationships among the conduction switch, commutation error and commutation information (delayed or advanced commutation) are shown in Table II.

### C. Phase Deviation $\beta$

In this paper, the actual back-EMF waveforms are measured offline by a constant speed test of a BLDC motor and the phase deviation $\beta$ can be obtained from the measured back-EMF. Fig. 4 shows the assembly of the BLDC motor used in this study. Fig. 5 shows the corresponding back-EMF waveforms of a constant speed test of 1200r/min.

### D. Implementation of the Proposed Method

In general, accurate commutation instants are obtained by 30 electrical degrees delayed shift of ZCPs in the sensorless drive technique and reactivating the motor windings in accordance with a predefined commutation sequence. The predefined commutation sequences are shown in Table III, where $\hat{H}_a$, $\hat{H}_b$ and $\hat{H}_c$ are the virtual hall signals.

When the motor rotates anti-clockwise, the commutation error $\phi$ can be rewritten as:

$$\phi=(-1)^{\left(\hat{H}_a+\hat{H}_b+\hat{H}_c\right)}\cdot\varphi\cdot 180/\pi \tag{25}$$

Table II shows that when the phase current flows in a different direction, the sign of the commutation error $\varphi$ obtained with the same function is opposite. After transformation using (25), the commutation error $\phi$ under delayed and advanced commutations is converted to positive and negative, respectively.

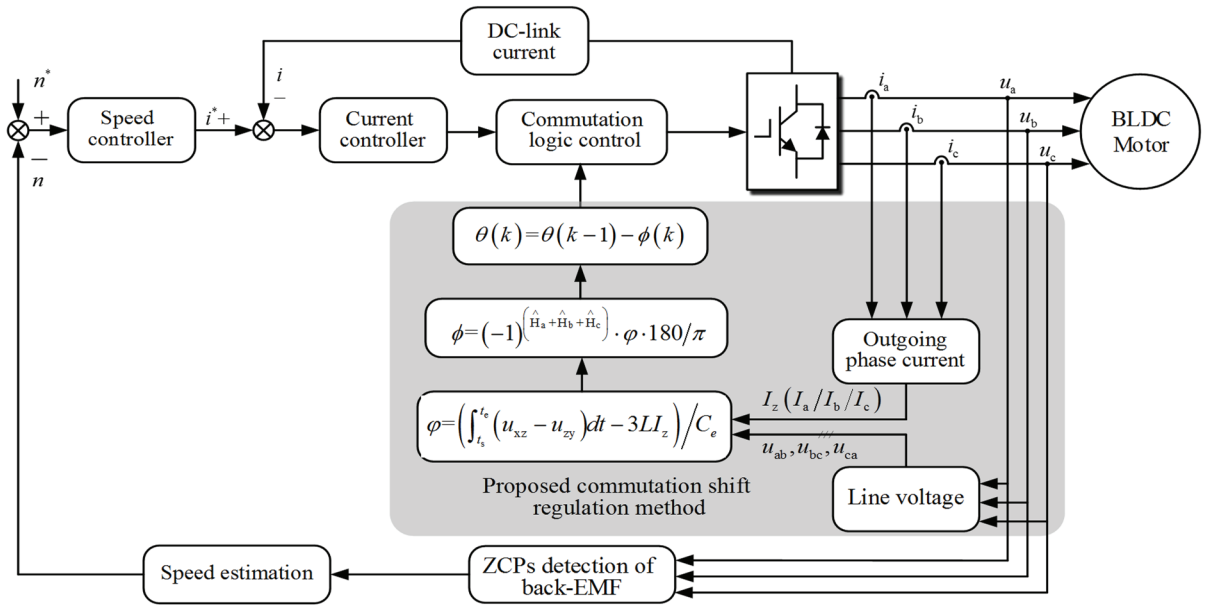


Fig. 6. Sensorless BLDC drive system with the proposed method.

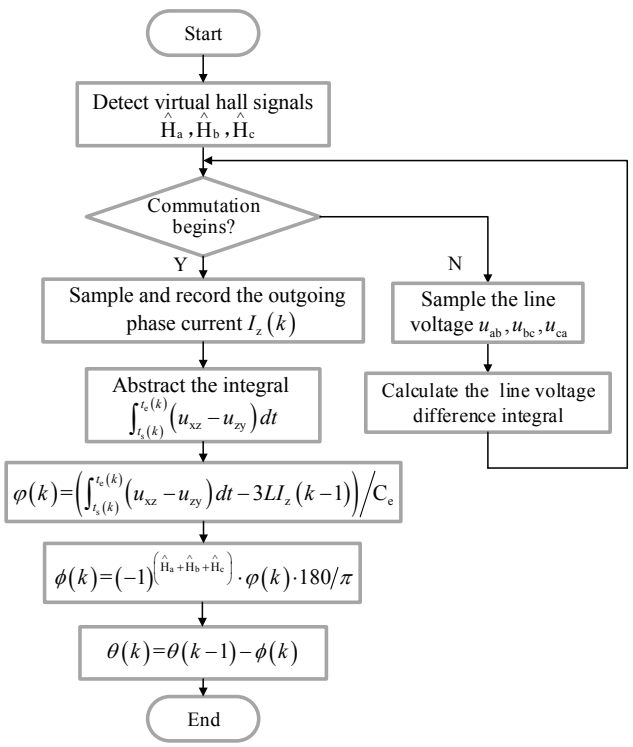


Fig. 7. Flowchart of the proposed regulation method.

Similarly, when the motor rotates clockwise, the commutation error $\phi$ can be shown as:

$$\phi=(-1)^{\left(\hat{H}_a+\hat{H}_b+\hat{H}_c+1\right)}\cdot\varphi\cdot 180/\pi \tag{26}$$

Therefore, after the commutation error $\phi$ is detected, the commutation shift is updated as:

$$\theta(k)=\theta(k-1)-\phi(k) \tag{27}$$

where $k$ ($k>0$) is the number of iterations and $\theta$ (0)=30°.

Fig. 6 shows a block diagram of a sensorless BLDC motor drive system with the proposed method. The system contains a speed-loop controller, a current-loop controller, and the proposed commutation shift regulation method. In the proposed commutation shift regulation method, when commutation signals are detected, the final value of the outgoing phase current is sampled and the line voltage difference selected according to Table II is integrated. When commutation occurs again, the line voltage difference integral is recorded and the commutation error $\phi$ is calculated with the sampled current value and the line voltage difference integral. Meanwhile, the entire regulation process mentioned above is resumed. A flowchart of the proposed method is shown in Fig. 7.

## IV. Experimental Results

The experimental prototype is set up to verify correctness and effectiveness of the proposed method. The experimental platform, which consists of the control system and an experimental motor is shown in Fig. 8. The motor is connected to a generator by a flexible coupling. The rated parameters of BLDC motor under study are shown in Table IV.

In the experiment, a BLDC motor is coupled to a dc generator. The core processor is a digital signal processor TMS320F28335 with a 150MHz clock frequency, and the three phase inverter is an intelligent power module PM50RL1A060 (Mitsubishi). The line voltage and phase current are sampled by a voltage sensor (LV25-P) and a current sensor (LTS15-NP), respectively. The modulation method of three-phase inverter is PWM-ON, and the switching frequency

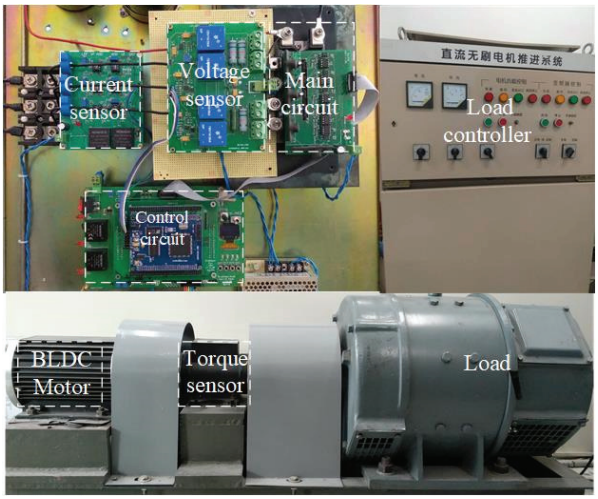


Fig. 8. Experimental setup of a BLDC motor drive system.

TABLE IV
MOTOR PARAMETERS

| Motor Parameter | Values |
|---|---|
| Rated voltage | 200V |
| Rated power | 2.5 kW |
| Rated speed | 1200 r/min |
| Rated torque | 20 Nm |
| Pole pairs | 4 |
| Phase inductance | 1.234 mH |
| Phase resistance | 0.0654Ω |
| Back-EMF coefficient | 0.528V/(rad/s) |

of the three-phase inverter and the sampling frequency of the voltage are 10kHz and 200kHz, respectively. The experimental results are monitored and recorded by a digital oscilloscope DL750, and the integral of the line voltage difference is observed through a DAC.

Fig. 9 show the phase current and line voltage difference integral $\int_{t_s}^{t_e}\left(u_{xz}-u_{zy}\right)dt$ under the delayed, advanced and accurate commutation, respectively. In the experiment, the motor operates at a speed of 600r/min and a torque load of 5.2 Nm. In addition, the commutation instants are set to be advanced or delayed by 10°. For analysis, the conduction period of $VT_3$ and $VT_2$ is taken as an example. The outgoing phase current $I_a$ before commutation and the line voltage difference integral $\int_{t_s}^{t_e}\left(u_{ca}-u_{ab}\right)dt$ are marked in circles. As seen in Fig. 9, the line voltage difference integral $\int_{t_s}^{t_e}\left(u_{ca}-u_{ab}\right)dt$ is different under delayed, advanced and accurate commutation. The absolute value of the integral under delayed and advanced commutation is higher than that under accurate commutation. Inaccurate commutation signals produce differences in the line voltage difference integral $\int_{t_s}^{t_e}\left(u_{xz}-u_{zy}\right)dt$ and the outgoing phase current $I_z$ before

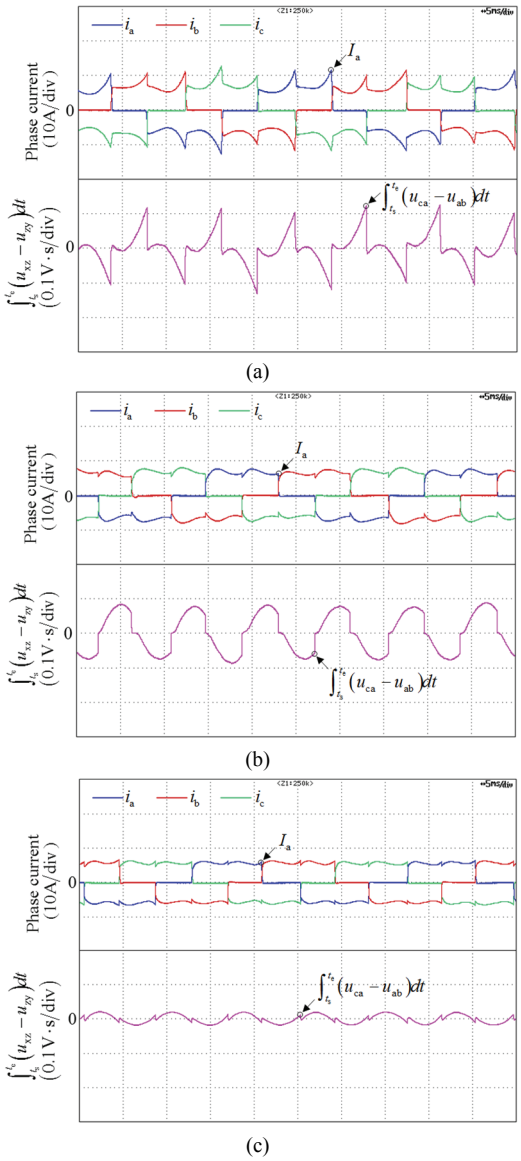


Fig. 9. Phase Current and integral of the line voltage difference. (a) Delayed commutation. (b) Advanced commutation. (c) Accurate commutation.

commutation. Experimental results show that the relationship between the voltage integral and the phase current before commutation can reflect commutation information.

Fig. 10 and Fig. 11 show phase current waveforms before and after regulation at speeds of 600 r/min and 1200r/min, respectively, where the hall signal $L_h$, the equivalent commutation signal $L_t$ (the equivalent commutation signal is synthesized from three virtual hall signals and its frequency is tripled, where $L_t=\hat{H}_a+\hat{H}_b+\hat{H}_c$ ), and the sensorless commutation signal $L_s$ are displayed. In Fig. 10 and Fig. 11, the commutation instants are advanced and delayed by approximately 10° before the proposed regulation method is employed, and the phase current $i_b$ under advanced and delayed commutations fluctuates upwards due to the commutation error. After completing the regulation, the current

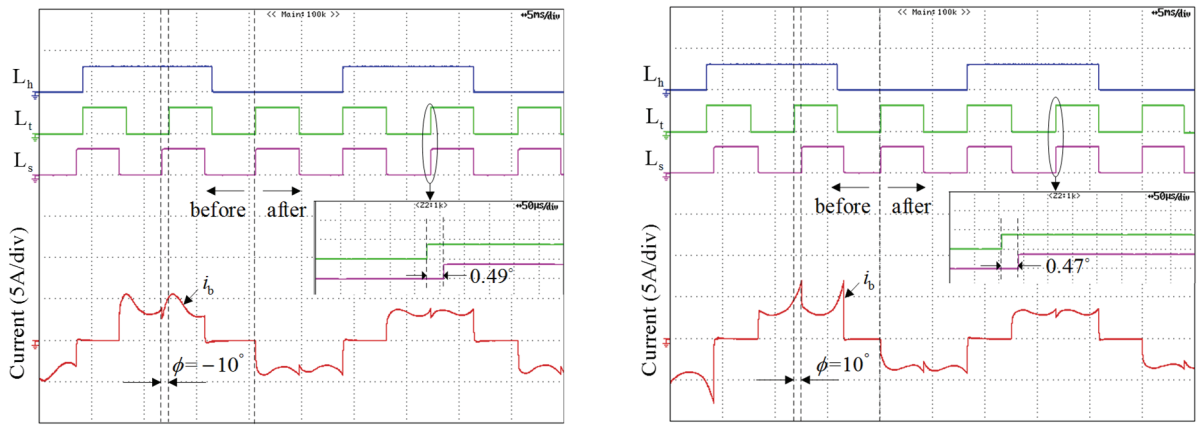


Fig. 10. Phase current waveforms before and after regulation. (a) Advanced commutation at a speed of 600r/min and a load torque of 2.5 Nm. (b) Delayed commutation at a speed of 600r/min and a load torque of 2.5 Nm.

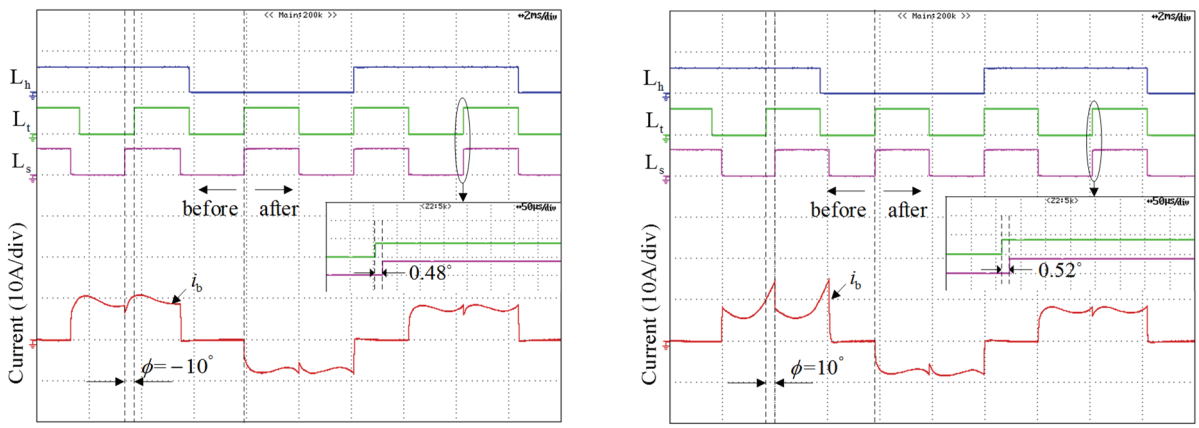


Fig. 11. Phase current waveforms before and after regulation. (a) Advanced commutation at a speed of 1200r/min and a load torque of 7 Nm. (b) Delayed commutation at a speed of 1200r/min and a load torque of 7 Nm.

ripple is effectively decreased. The adjustment accuracy of the proposed method is tested and the obtained results are shown in the enlarged view. As seen in the enlarged views, the errors are about 5% when compared with the equivalent commutation signal $L_t$. Therefore, the proposed method can regulate commutation instants accurately in steady speed operation.

The torque ripple is defined as follows:

$$K_r = \frac{T_{P\text{-}P}}{T_{avg}}$$

where $T_{P\text{-}P}$ is the peak-peak value of the torque, and $T_{avg}$ is the average value of the torque.

Fig. 12 and Fig. 13 show speed and torque waveforms under different conditions. As can be seen in these figures, the speed ripple is not obvious under these two operating conditions. When the motor runs at a speed of 600r/min and a load torque of 7 Nm, the torque ripples $K_r$ are 17.1%, 15.3% and 13.8% under advanced, accurate and delayed commutations, respectively. When the motor runs at a speed of 1200r/min and a load torque of 11Mn, the torque ripples $K_r$ are 26.1%, 9.5% and 8.9% under advanced, accurate and delayed commutations, respectively. It is found that the torque ripple under accurate commutation is lower than that under advanced commutation, but higher than that under delayed commutation. When delayed commutation occurs, the current ripple of un-commutated phase current is reduced, which results in a lower torque ripple than that under accurate commutation. Specific reasons for this are provided in [26].

To test the convergence rate of the proposed method in steady speed operation, the phase difference between the sensored signals and the sensorless commutation signals is set to about 10°, and the motor operates at a speed of 800r/min and a load torque of 3.5 Nm. Fig. 14 shows the phase current, the line voltage difference integral and their enlarged views with the proposed method. Before the point of $s_1$, the phase current $i_b$ curls up, and the integral $\int_{t_s}^{t_e}(u_{xz}-u_{zy})dt$ is high. When the regulation method is activated at the point of $s_1$, the phase current pulsation decays rapidly, the integral

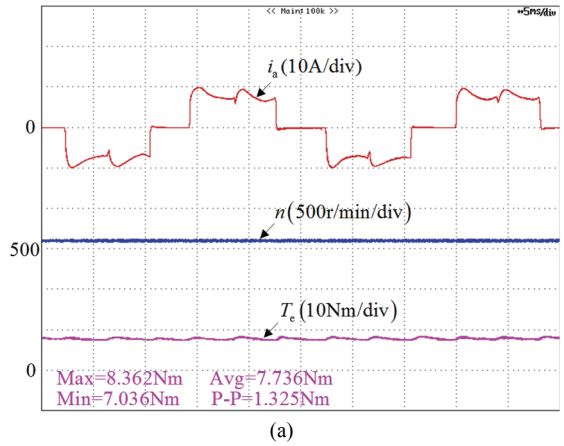


(a)

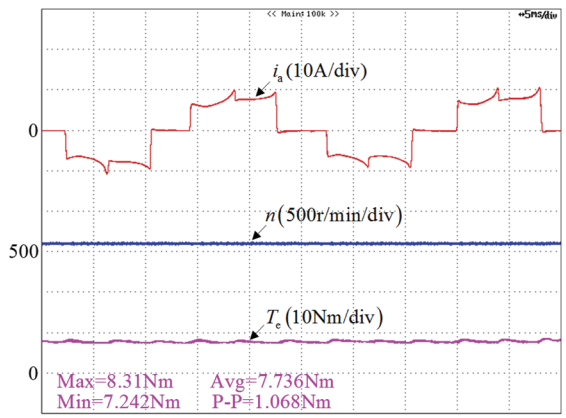


(b)

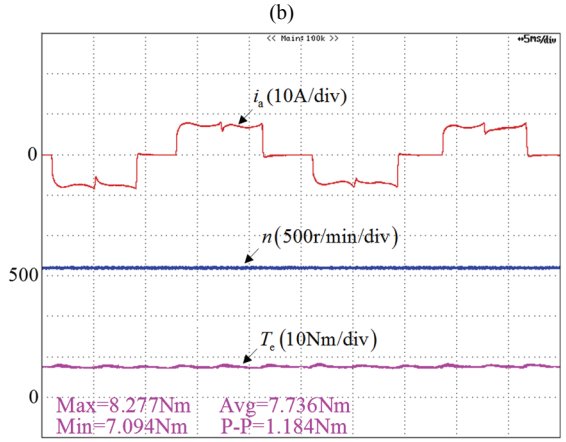


(c)

Fig. 12. Speed and torque waveforms under different conditions. (a) Advanced commutation at a speed of 600r/min and a load torque of 7 Nm. (b) Delayed commutation at a speed of 600r/min and a load torque of 7 Nm. (c) Accurate commutation at a speed of 600r/min and a load torque of 7 Nm.

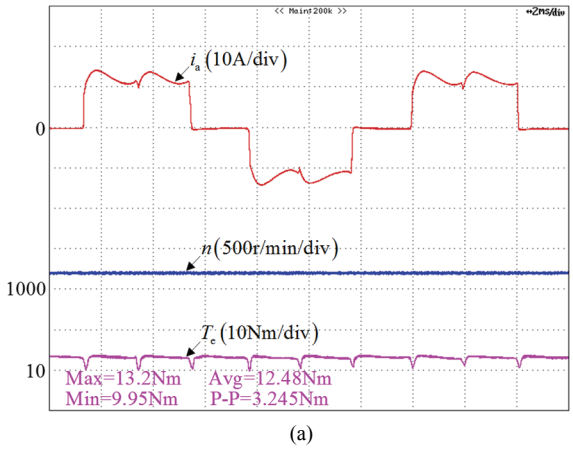


(a)

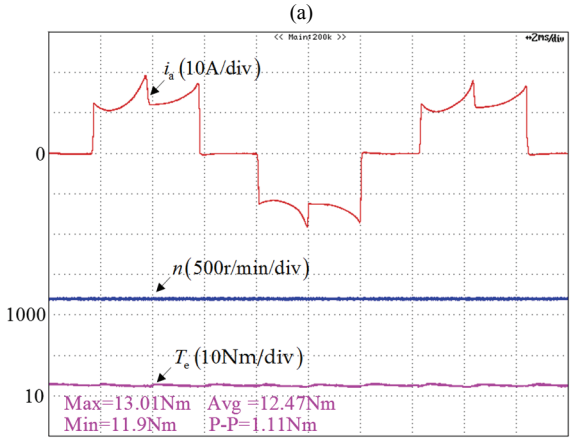


(b)

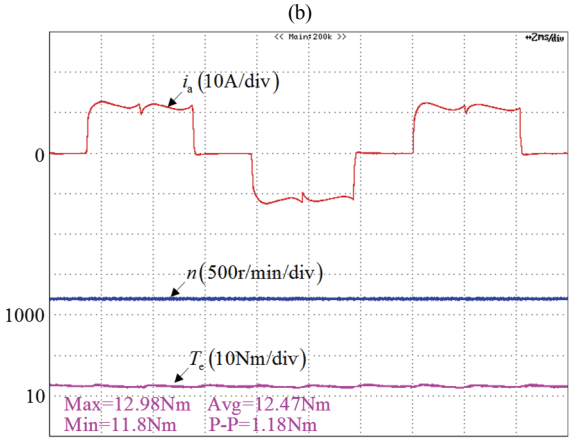


(c)

Fig. 13. Speed and torque waveforms under different conditions. (a) Advanced commutation at a speed of 1200r/min and a load torque of 11 Nm. (b) Delayed commutation at a speed of 1200 r/min and a load torque of 11 Nm. (c) Accurate commutation at a speed of 1200r/min and a load torque of 11 Nm.

$\int_{t_s}^{t_e}\left(u_{xz}-u_{zy}\right)dt$ becomes lower, and the commutation error converges to zero within 4.68ms. In addition, the convergence rate of the proposed method at different speeds is tested and shown in Table V. The obtained test results show that the proposed method converges rapidly in a wide speed range.

Subsequently, the performance of the proposed method during the transient process is tested. In the experiment, the commutation instants are delayed by approximately 12°, and the motor is accelerated from 300 r/min to 1200r/min with a load torque of 8Nm. Fig. 15 shows the motor speed, phase current, the integral of the line voltage difference and their enlarged views with the proposed method. When the motor speed ramps up, the regulation method is initiated at the points of $s_1$ and $s_2$, and is terminated at the points of $t_1$ and $t_2$. As shown in Fig. 15, after the regulation method is activated,

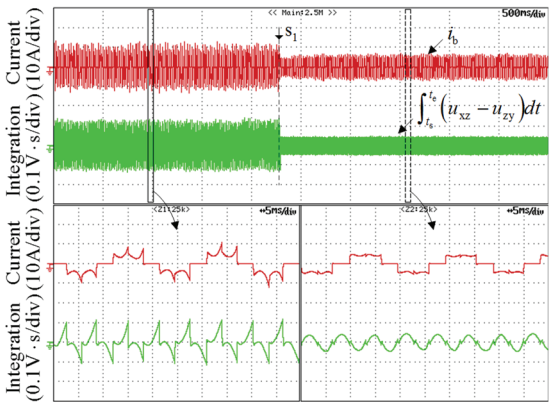


Fig. 14. Comparative results of the phase current, the integral and their enlarged views at a speed of 800r/min and a load torque of 3.5 Nm with the proposed method.

TABLE V
CONVERGENCE RATE OF THE PROPOSED METHOD

| Speed (r/min) | 300 | 500 | 800 | 1000 | 1200 |
|---|---|---|---|---|---|
| Proposed method(ms) | 12.5 | 7.5 | 4.68 | 3.75 | 3.13 |

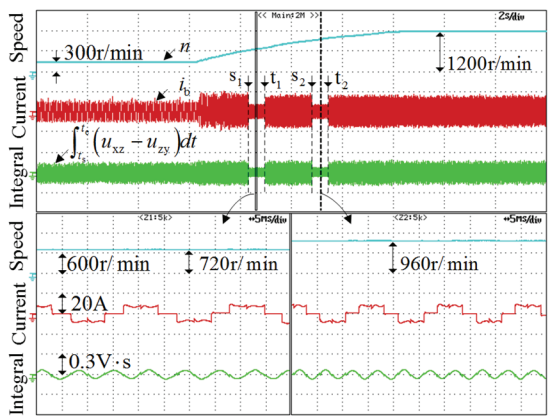


Fig. 15. Transient performance and enlarged views with the proposed method when the motor accelerates from 300r/min to 1200r/min.

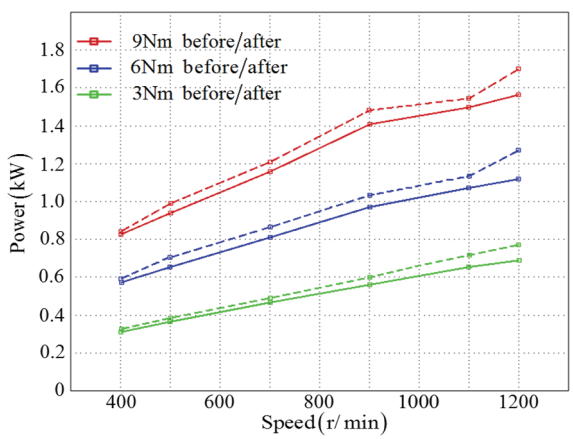


Fig. 16. Motor power consumption comparison between a system with and without the proposed method.

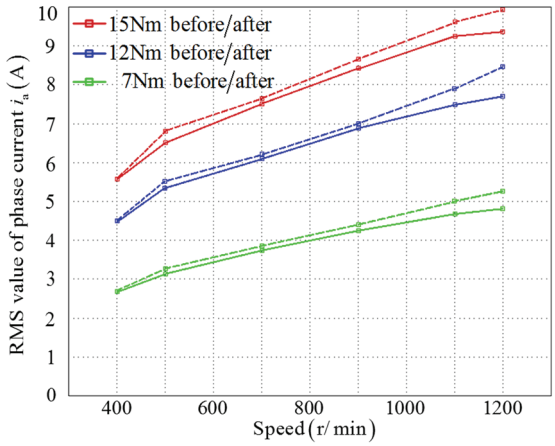


Fig. 17. Comparison of the RMS values of phase current between a system with and without the proposed method.

the current fluctuation is effectively decreased, and the phase current appears symmetrical and flat. The proposed regulation method exhibits satisfactory dynamic performance in the variable speed operation.

Moreover, the power consumption and the RMS value of the phase current are reduced after the commutation instants are regulated with the proposed method. The power consumption is tested by calculating it as the product of the dc-bus voltage and the dc bus current. Fig. 16 and Fig. 17 show the power consumption and the RMS value of the phase current of a BLDC motor with and without regulation after steady operation for 40 min, respectively. In addition, the speed range is from 400r/min-1200r/min under different loads. The dotted and solid lines represent the results before and after regulation, respectively. The experimental results in Fig. 16 and Fig. 17 indicate that the proposed method can effectively reduce the power consumption and RMS value of phase current over a wide speed range, especially in the high-speed range.

## V. CONCLUSIONS

This paper proposes a fast regulation method for the commutation shift of sensorless BLDC motor drive systems. The commutation error is directly calculated with the line voltage difference integral of 60 electrical degrees and the outgoing phase current before commutation. In addition, it is used to regulate commutation shift, which results in a faster convergence rate of the commutation error. The impact of phase inductance freewheeling is considered during the solution of the commutation error, and the detection precision of the commutation error is improved accordingly. The commutation error features positive and negative polarity, and the commutation information can be judged immediately. Finally, the effectiveness and feasibility of the proposed regulation method are verified through experiments. The experimental results show that the proposed method can

accurately regulate commutation instants and effectively reduce energy loss.

## REFERENCES


[1] K. Y. Cheng and Y. Y. Tzou, "Design of a sensorless commutation IC for BLDC motors," *IEEE Trans. Power Electron*., Vol. 18, No. 6, pp. 1365-375, Nov. 2003.

[2] J. Fang, X. Zhou, and G. Liu, "Precise accelerated torque control for small inductance brushless DC motor," *IEEE Trans. Power Electron.*, Vol. 28, No. 3, pp. 1400-412, Mar. 2013.

[3] T. H. Kim and M. Ehsani, "Sensorless control of BLDC motors from near-zero to high speeds," *IEEE Trans. Power Electron.*, Vol. 19, No. 6, pp. 1635-645, Nov. 2004.

[4] N. Urasaki, T. Senjyu, K. Uezato, and T. Funabashi, "Adaptive dead-time compensation strategy for permanent magnet synchronous motor drive," *IEEE Trans. Energy Convers*., Vol. 22, No. 2, pp. 271-280, Jun. 2007.

[5] M. Bertoluzzo, G. Buja, R. K. Keshri, and R. Menis, "Sinusoidal versus square-wave current supply of PM brushless DC drives: A convenience analysis," *IEEE Trans. Ind. Electron.*, Vol. 62, No. 12, pp. 7339-7349, Dec. 2015

[6] F. G. Capponi, G. D. Donato, L. D. Ferraro, O. Honorati, M. C. Harke, and R. D. Lorenz, "AC brushless drive with low-resolution hall-effect sensors for surface-mounted PM machines," *IEEE Trans. Ind. Appl*., Vol. 42, No. 2, pp. 526-535, Mar./Apr. 2006.

[7] T. W. Chun, Q. V. Tran, H. H. Lee, and H. G. Kim, "Sensorless control of BLDC motor drive for an automotive fuel pump using a hysteresis comparator," *IEEE Trans. Power Electron.*, Vol. 29, No. 3, pp. 1382-1391, Mar. 2014.

[8] J. Shao, D. Nolan, M. Teissier, and D. Swanson, "A novel microcontroller-based sensorless brushless dc (BLDC) motor drive for automotive fuel pumps," *IEEE Trans. Ind. Appl.*, Vol. 39, No. 6, pp. 1730-1740, Nov./Dec. 2003.

[9] Q. Jiang, C. Bi, and R. Huang, "A new phase-delay-free method to detect back EMF zero-crossing points for sensorless control of spindle motors," *IEEE Trans. Magn.,* Vol. 41, No. 7, pp. 2287-2294, Jul. 2005.

[10] W. Li, J. Fang, and H. Li, "Position sensorless control without phase shifter for high-speed BLDC motors with low inductance and non-ideal back EMF," *IEEE Trans. Power Electron.*, Vol. 31, No. 2, pp.1354-1366, Feb. 2016.

[11] J.-W. Park, S.-H. Hwang, and J.-M. Kim, "Sensorless control of brushless DC motors with torque constant estimation for home appliances," *IEEE Trans. Ind. Appl.*, Vol. 48, No. 2, pp. 677-683, Mar./Apr. 2012.

[12] S. Wang and A. Lee, "A 12-step sensorless drive for brushless DC motors based on back-EMF differences," *IEEE Trans. Energy Convers.*, Vol. 30, No. 2, pp. 646-654, Jun. 2015.

[13] Z. Qiao, T. Shi, Y. Wang, Y. Yan, C. Xia, and X. He, "New sliding-mode observer for position sensorless control of permanent-magnet synchronous motor," *IEEE Trans. Ind. Electron.*, Vol. 60, No. 2, pp. 710-719, Feb. 2013.

[14] Y. Zhao, W. Qiao, and L. Wu, "An adaptive quasi-sliding-mode rotor position observer-based sensorless control for interior permanent magnet synchronous machines," *IEEE Trans. Power Electron.*, Vol. 28, No. 12, pp. 5618-5629, Dec. 2013.

[15] F. Alonge, F. D'Ippolito, and A. Sferlazza, "Sensorless control of induction-motor drive based on robust Kalman filter andadaptive speed estimation," *IEEE Trans. Ind. Electron.*, Vol. 61, No. 3, pp. 1444-1453, Mar. 2014.

[16] M. Barut, S. Bogosyan, and M. Gokasan, "Experimental evaluation of braided EKF for sensorless control of induction motors," *IEEE Trans. Ind. Electron.*, Vol. 55, No. 2, pp. 620-632, Feb. 2008.

[17] I. Bahri, L. Idkhajine, E. Monmasson, and M. E. Amine Benkhelifa, "Hardware/software codesign guidelines for system on chip FPGA-based sensorless ac drive applications," *IEEE Trans. Ind. Informat.*, Vol. 9, No. 4, pp. 2165-2176, Nov. 2013.

[18] P. Mercorelli, "A hysteresis hybrid extended kalman filter as an observer for sensorless valve control in camless internal combustion engines," *IEEE Trans. Ind. Appl.*, Vol. 48, No. 6, pp. 1940-1949, Nov./Dec. 2012.

[19] P. Mercorelli, "A two-stage augmented extended kalman filter as an observer for sensorless valve control in camless internal combustion engines," *IEEE Trans. Ind. Electron.*, Vol. 11, No. 59, pp. 4236-4247, Nov. 2012.

[20] H. C. Chen and C. M. Liaw, "Sensorless control via intelligent commutation tuning for brushless dc motor," *Inst. Electron. Eng. Electron. Power Appl.,* Vol. 146, No. 6, pp. 678-684, Nov. 1999.

[21] J. Fang, W. Li, and H. Li, "Self-compensation of the commutation angle based on dc-link current for high-speed brushless DC motors with low inductance," *IEEE Trans. Power Electron.*, Vol. 29, No. 1, pp. 428-439, Jan. 2014.

[22] X. Wu, B. Zhou, F. Song, F. Chen, and J. Wei, "A closed loop control method to correct position phase for sensorless Brushless DC motor," *in Conference on Electrical Machines and Systems,* Vol. 6, pp. 1460-1464, 2008.

[23] G.H. Jang and M.G. Kim, "Optimal commutation of a BLDC motor by utilizing the symmetric terminal voltage," *IEEE Trans. Magn.*, Vol. 42, No. 10, pp. 3473-3475, Oct. 2006.

[24] X. Yao, J. Zhao, G. Luo, H. Lin and J. Wang, "Commutation Error Compensation Strategy for Sensorless Brushless DC Motors," *Energies*, Vol. 12, No. 2, Jan. 2019.

[25] P. Damodharan, R. Sandeep and K. Vasudevan. "Simple position sensorless starting method for brushless DC motor," *IET Electric Power Appl.*, Vol. 2, No. 1, pp. 49-55, Jan. 2008.

[26] X. Yao, X. Jiang, Y. Zhang, Y. Yang, and J. Chang, "A novel method based on delaying Hall signal for reducing torque ripple of brushless DC motor," in *Conf. IECON 2016*, pp. 2642-2647, 2016.


**Xuliang Yao** received his Ph.D. degree from the College of Automation, Harbin Engineering University, Harbin, China, in 2005. He is presently working as a Professor in the College of Automation, Harbin Engineering University. His current research interests include power electronics and power drives, ship electric propulsion, and control theory of shipping motion.

**Jicheng Zhao** received his B.S. and M.S. degrees from the College of Automation, Harbin Engineering University, Harbin, China, in 2008 and 2011, respectively. He is presently working towards his Ph.D. degree in the College of Automation, Harbin Engineering University. His current research interests include sensorless drives and commutation ripple suppression of BLDC motors.

**Jingfang Wang** was born in Hebei, China, in 1984. He received his B.S. degree in Automation from Yanshan University, Qinhuangdao, China, in 2008; his M.S. degree in Electrical Engineering from the Harbin Engineering University, Harbin, China, in 2012; and his Ph.D. degree in Electrical Engineering from the Harbin Institute of Technology, Harbin, China, in 2017. Since 2017, he has been working as a Lecturer in the College of Automation, Harbin Engineering University. His current research interests include high power converters and harmonics compensation.